Partially Metal-Coated Tips for Near-Field Nanospectroscopy

Yujia Zhang, Xinzhong Chen, Derek Chen, Ziheng Yao, Suheng Xu, Patrick McArdle, M. Mumtaz Qazilbash, and Mengkun Liu

Partially metal–coated Tips for Near-field Nanospectroscopy

Yujia Zhang[1,2,3*], Xinzhong Chen[1], Derek Chen[1], Ziheng Yao[1,4], Suheng Xu[1,5], Patrick McArdle[6], M. Mumtaz Qazilbash[6] and Mengkun Liu[1,7*]

[1]Department of Physics and Astronomy, Stony Brook University, Stony Brook, New York 11794, USA

[2]State Key Laboratory of Transducer Technology, Shanghai Institute of Microsystem and Information Technology, Chinese Academy of Sciences, Shanghai 200050, China

[3]School of Graduate Study, University of Chinese Academy of Sciences, Beijing 100049, China

[4]Advanced Light Source Division, Lawrence Berkeley National Laboratory, Berkeley, California, 94720, USA

[5]Department of Physics, Columbia University, New York 10027, USA

[6]Department of Physics, College of William & Mary, Williamsburg, VA 23187-8795, USA

[7]National Synchrotron Light Source II, Brookhaven National Laboratory, Upton, New York 11973, USA

*yujia.zhang@stonybrook.edu; yoga@mail.sim.ac.cn;

*mengkun.liu@stonybrook.edu

Abstract

Scanning probes with functional optical responses are key components of scanning near-field optical microscopes. For nanospectroscopy performed at infrared (IR) and terahertz (THz) frequencies, one major challenge is that the commonly used metal-coated silicon tips yield nonadjustable coupling efficiency across the spectrum, which greatly limits the signal-to-noise ratio. Here, we test the possibility of a generic design scheme for wavelength-selective tip enhancement via finite-element numerical modeling. We employ a Si-based tip with various gold coating lengths on the top, yielding a customizable near-field field strength at the tip apex. Calculations show a wavelength-dependent enhancement factor of the metal-coated tip due to the geometrical antenna resonances, which can be precisely tuned throughout a broad spectral range from visible to terahertz frequencies by adjusting the length of the metal coating. By changing the coating pattern into a chiral helical structure on an achiral tip, we also demonstrate the importance of coating-length effect in designing high-performance enantiomeric near-field scanning. Our methods and findings offer interesting perspectives for developing near-field optical probes, pushing the detection and resolution limits of tip-enhanced near-field detections such as fluorescence, Raman, IR, and THz nanospectroscopies.

Introduction

Scattering-type scanning near-field optical microscope (s-SNOM) typically utilize metal or metal-coated atomic force microscope (AFM) tips as the scattering near-field probe.[1, 2] The tips are usually 10 to 15 μm long for infrared (IR) s-SNOM and 50 to 200 μm long for terahertz (THz) s-SNOM.[3-5] The fixed tip length raises considerable issues since it yields different near-field enhancement factors for different incident wavelengths. This is one of the major reasons that near-IR and THz s-SNOM have low signal to noise ratio compared to the mid-IR s-SNOM; the tip length is not ideal for the field enhancement.[6] Moreover, in order to yield the best coupling coefficient, the cone-shape tip structure also requires the incident light to be linearly polarized with respect to the symmetric tip axis.[2, 7]

Previous studies used tips with different configurations to substantially improve the topographical and optical resolution via, for example, multiwalled carbon nanotubes and high-aspect ratio gold cones with a fixed Si base or cantilever.[8-10] While these studies have shown the evidence of enhanced near-field signals in certain specific cases, broad spectral responses have not been fully achieved yet. Specifically designed probe geometries such as one-dimensional gratings and chiral grooves have also been utilized to break the tip symmetry and adapt with unaligned polarized light.[11-13] These approaches achieved significant advances, but

the tip geometry engineering is not a straightforward task. Methods for convenient tuning of the light-tip interaction are still in need.

Here we propose an easy to implement method, by partially coating metal on standard Si AFM tip, to induce customizable broad-spectrum antenna effect and enhance the field at the tip apex. We thoroughly study the influence of the coating-length effect (CLE) on the near-field enhancement using finite-element numerical modeling.[14-16] The merit of partially-metal–coated tip is that it can be widely used for near-field nanospectroscopy at different incident wavelengths while maintaining the same tip base design. The partial coating method can also be engineered and applied to create chiral structures, so that the tip is sensitive to the chirality of the incident light.

Methods

Numerical Simulations. The numerical simulations were conducted using the commercial software COMSOL Multiphysics 5.4 (Stockholm, Sweden) based on surface-based finite element methods in the frequency domain. The tip was modeled as a conical frustum and a hemispherical apex with geometric parameters given in Figure 1a. The cone angle θ is 30° and the tip end is modeled as a hemisphere with radius r = 50 nm. This geometry resembles that of commercially available AFM tips, which are typically used in s-SNOM experiments. For the tip, every boundary was modeled by impedance boundary conditions in order to save computer memory with the frequency-dependent dielectric constants of Au and Si, respectively.[17, 18] Moreover, at the mid-IR range, the skin depth of Au is around 10 to 20 nm.[2] Hence, we set the Au coating as 50 nm thick throughout our simulations to reduce the influence of coating thickness to the minimal level. In order to properly describe the near-field illumination, we applied the scattered field formulation, in which the field is split into an illumination field (also referred to as a background field) and a scattered field that we analyzed in this work. We use p-polarized plane wave illumination (electric field E_{inc}) at an incident angle of 60° relative to the tip axis with the wavelength ranging from near/mid-IR range (λ= 0.632 to 30 μm) to THz range (λ = 30 to 3000 μm). Without losing generality, E_{norm} at 20 nm directly above the tip apex is used for evaluating the near-field enhancement.[2] Verification simulations were performed using the commercial software Altair FEKO 2020 based on the method of moments using the surface equivalence principle, with the tip geometry and source settings following the COMSOL simulations. Coarse mesh settings were used to reduce simulation time; to maintain the accuracy of the simulation despite these settings, a spherical region of refined mesh was defined around the tip apex, with a mesh size of 25 nm for both the mid-IR and THz models.

Results

To elucidate the effect of the tip-coating length to the near-field enhancement at different incident wavelengths, we first perform numerical full-wave simulations (see Methods) of IR-/THz-illuminated tips with conical geometry depicted in Figure 1a. A standard high resistive Si AFM tip with the total shank length of L is partially coated by Au at the tip apex with a coating length of l. L is fixed at 20 μm for near/mid-IR range and 200 μm for THz range simulation throughout this article. With the coating length ratio ($\frac{l}{L}$) varying, the corresponding normalized electric near-field (E_{norm}) at the tip apex can be recorded as a function of the incident wavelength.

Figure 1b presents the electric field distribution of a specific case ($\frac{l}{L}$ = 0.5, light wavelength = 200 μm), showing the field around the tip apex with a maximum 80-fold enhancement. Compared to pure Au tips of the same Au length (l) but without the Si base (Figure 1c), the partially coated tips greatly boost the near-field enhancement at all wavelengths.[10] Since the Au parts are the same, the enhancement comes from the resonance effect of the additional Si base in the Au/Si case. First, the E_{norm} is amplified at the initial peak wavelength around $2l$ (~4 μm for l = 2 μm and ~40 μm for l = 20 μm) for both mid-IR and THz range (Figure 1d and Figure S1 in the Supplemental Material).[17] Interestingly, when the wavelength is far beyond the length of l (more than 5 times), the spatial mismatch between wavelength and Au length would severely decrease the E_{norm} of standard fully metalized AFM tips. However, the partially coated tips still preserve the strong enhancement throughout the broad spectral range. Considering some previous works have mentioned that the tip−sample near-field interaction is not only influenced by near-field enhancement but also depends on the optical properties of the sample, here we exclude the samples to avoid extra complexity in our models.[18]
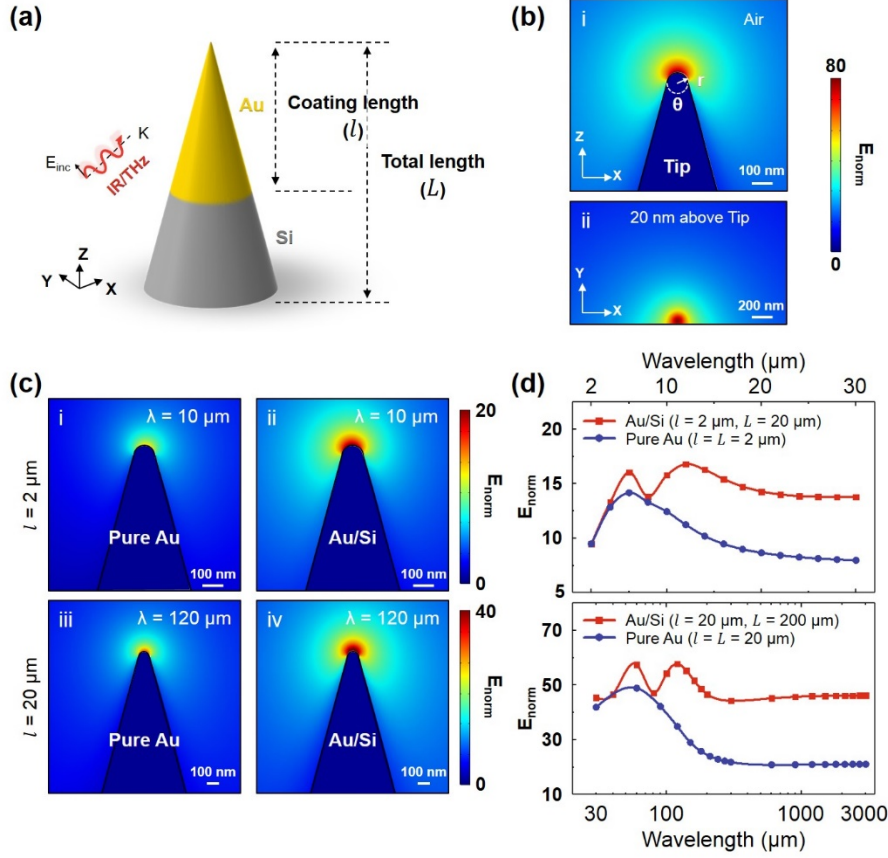
Figure 1. Numerical modeling of the resonant antenna probe based on partially coated AFM tip for near-field nanospectroscopy. (**a**) Schematic of the numerical model to simulate the near-field enhancement at the tip apex for different Au length (l) coated on a Si tip with a fixed total length (L). (**b**) The numerically calculated E_{norm} distribution around the apex of a half-coated 200 μm long antenna tip under the illumination of THz light (wavelength of 200 μm). The upper image i) shows the side view of the near-field distribution and the lower image ii) shows the top view at 20 nm above half of the tip apex. The E_{norm} is normalized to the incident electric field (E_{inc}), which is linearly polarized at a 60-degree angle with respect to the tip axis. (**c**) The numerically calculated E_{norm} distribution around the apex of a fully coated pure Au tip (i and iii) and a partially coated Au/Si tip (ii and iv). The Au lengths l of the two types of tips are the same, with 2 μm length in mid-IR range (i and ii) and 20 μm length in THz range (iii and iv). (**d**) The E_{norm} of the two types of tips for illuminating light wavelength set to mid-IR range (top) and THz range (bottom).

Next we present the coating length dependent near-field enhancement in near/mid-IR range. In Figure 2a, we plotted the two-dimensional color map of E_{norm} versus the incident wavelength and length ratio. Noticeably, the E_{norm} mapping shows two resonating frequency ranges, one ranging from 4 to 8 μm while the other ranging from 10 to 30 μm. The low-wavelength resonance occurs when the length ratio $\frac{l}{L}$ varies between 0.1 and 0.3, showing E_{norm} higher than that at larger length ratios (around 1.5 times for 8 μm incident wavelength, Figure 2b). Importantly, this enhancement results from relatively short coating length, indicating that for incident light at 4 ~ 8 μm, the partially coated tip can potentially provide a better electric near-field signal.[19] To further validate this advantage of the CLE, we compared the E_{norm} of partially coated tip with pure Au tip. As shown in Figure

S1, for tip length shorter than 8 μm, partially coated tip shows a remarkable increase of E_{norm} compared to the pure Au tip. The difference gradually decreases to zero when the coating ratio further increases to 1, which can be explained by the proportional change of the conductive Au coating and capacitive Si base, as will be discussed in detail later.

The second resonance range starts at 10 μm and reaches the resonant peak with a relatively flat trend (Figure 2b, 2c, S2 and S3 in the Supplemental Material).[17] Interestingly, we found the resonant peak frequency is related to the length ratio of the tip (red dotted line marked in Figure 2c). This nonlinear dependence can be understood analogously to dipolar and conical radio wave antennas.[2, 10] This CLE induced spectral shift can be simplified as a serial connection of impedances given by $Z_{tip} = Z_{Au} + Z_{Si}$, where the Z_{tip} is the impedance of the whole tip, Z_{Au} and Z_{Si} the impedance of Au coating and dielectric Si base. According to reported antenna theory, the resonant wavelength of dipolar antenna is close to $\frac{2l}{n}$ with n being the resonance order.[20, 21] Similarly, for Z_{Au}, the resonance wavelength of the Au coating should shift to longer values when the coating length increases.[22] At the same time, the increased coating length decreases the area of the exposed Si base and decreases the active capacitive load Z_{Si}, which also redshifts the antenna resonance.[23] Since the maximum E_{norm} depends on the induced optical displacement current, the amplitude of E_{norm} is related to the value of Z_{tip}.[24] Because the dielectric Z_{Si} is much larger than conductive Z_{Au}, the overall Z_{tip} decreases and the maximum E_{norm} increases as the coating length ratio goes up (Figure 2d). Therefore, the antenna changes from the dielectric-dominant resonance to the metallic-dominant resonance by increasing the coating length. During this transition, the Si base acts as a broadband antenna, especially in shorter wavelength range and smaller tip structure. Even for illumination at 632 nm, the CLE can still tune the near-field intensity at a relatively minor level, showing the feasibility of customizing the coating length according to different types of nanospectroscopy using the broad spectral range (Figure S4 in the Supplemental Material).[17, 25]
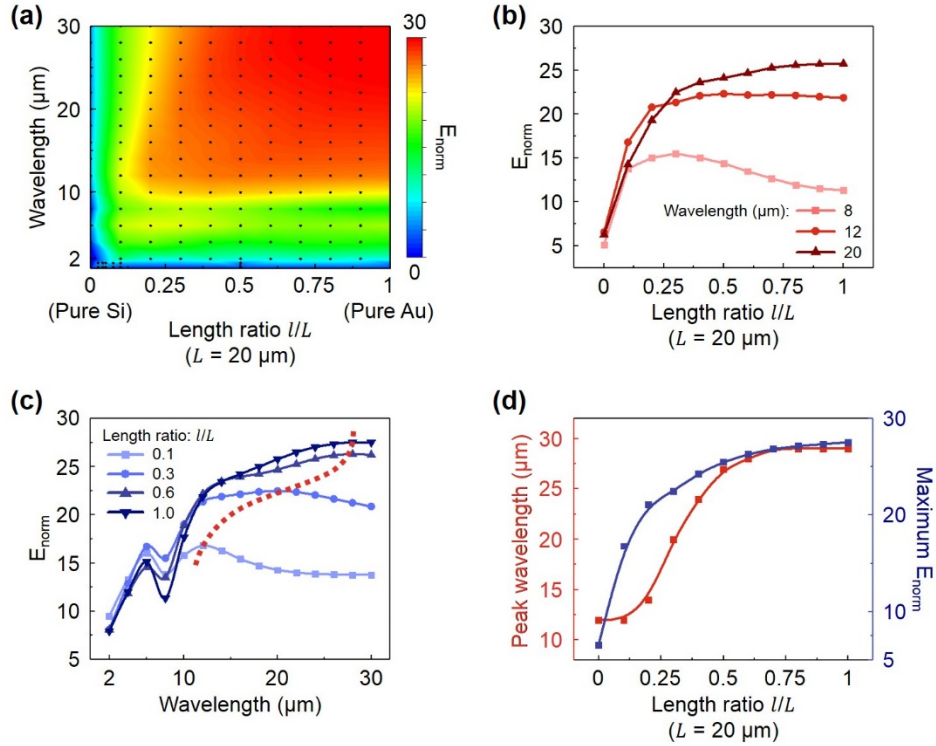
Figure 2. Simulation of the CLE in near/mid-IR range. (**a**) The near-field enhancement mapping for different length ratios with L fixed at 20 µm. The E_{norm} is calculated at 20 nm above the tip apex. (**b**) The horizontal line cuts of the mapping, showing the E_{norm} as a function of length ratio with different illuminating light wavelengths. (**c**) The vertical line cuts of the mapping, showing the E_{norm} as a function of illuminating light wavelength with different length ratios. The red dotted line marks the maximum E_{norm} point for each length ratio. (**d**) The wavelength and maximum E_{norm} of different length ratios corresponding to the red dotted line shown in (c), which is supplemented by a finer scan with smaller wavelength steps (Figure S2 in the Supplemental Material).[17]

In addition to the near/mid-IR range simulations, we also explored the CLE in THz range (Figure 3a). Comparing with Figure 2, similar structural dependent spectral responses were observed: first of all, the resonant peak still occurs at lower wavelength (60~80 µm) when the length ratio varies from 0.1 to 0.4, indicating the better performance of partially coated tip compared to pure metallic tip (see Figure S1 as well); moreover, the second major resonance raises from 100 µm and slowly decreases after 500 µm with a flat broadband near-field enhancement (Figure 3b and c). The long tail pattern over 500 to 3000 µm can be attributed to the gradually increased spatial mismatch (> 10 fold) between THz light and the fixed total length of coated tip (Figure 3c); for the near- and mid-IR simulations, this mismatch is relatively small, so the decay of the resonant peak is not as obvious. Importantly, the nonlinear relation between the second resonant wavelength and length ratio remains valid in the THz range (Figure 3d). The maximum E_{norm} gradually saturates as the length ratio increases to that of pure Au, while the corresponding peak wavelength follows the same trend in near/mid-IR range due to the decreased Z_{tip} and increased resonating Au length.
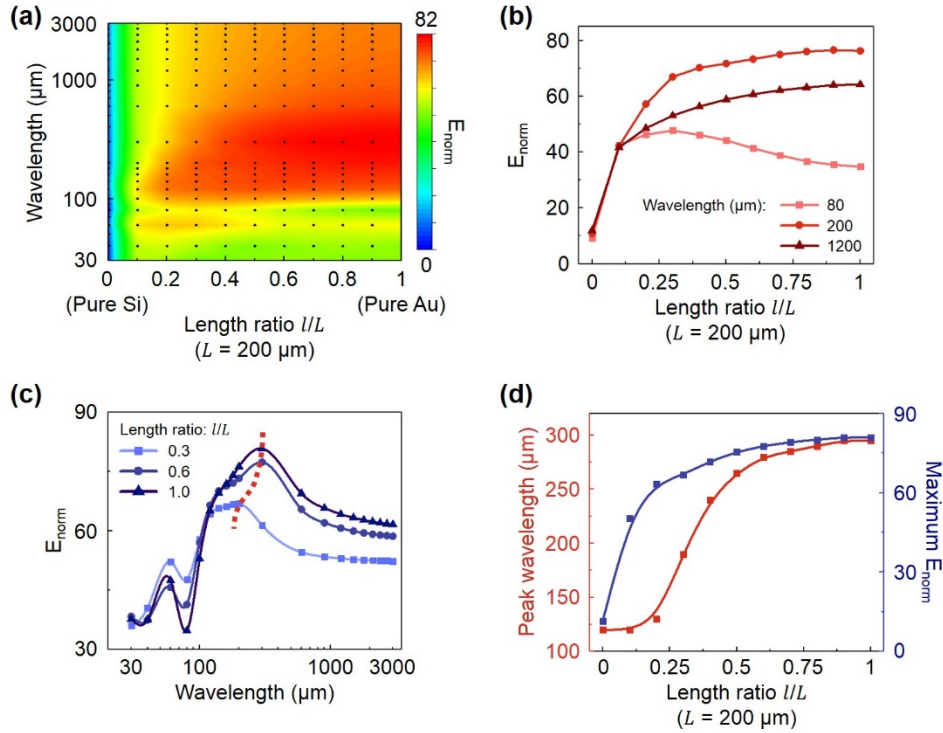
Figure 3. Simulation of the CLE in THz range. (**a**) The near-field enhancement mapping for different length ratios with L fixed at 200 μm. The E_{norm} is calculated at 20 nm above the tip apex. (**b**) The horizontal line cuts of the mapping, showing the E_{norm} as a function of length ratio with different illuminating light wavelengths. (**c**) The vertical line cuts of the mapping, showing the E_{norm} as a function of illuminating light wavelength with different length ratios. The red dotted line marks the maximum E_{norm} point for each length ratio. (**d**) The wavelength and maximum E_{norm} of different length ratios corresponding to the red dotted line shown in (c), which is supplemented by a finer scan with smaller wavelength steps (Figure S2 in the Supplemental Material).[17]

A more realistic tip geometry can be found in Figure 4a, where the metallic (Au) sample (case ii) and/or Si cantilever are included (case iii).[10] For the case ii (with substrate), we used the same Au as the tip with bulky structure ($12 \times 12 \times 1$ μm^3 for IR range and $120 \times 120 \times 10$ μm^3 for THz range) to eliminate structural effects on the signal enhancement. For the attached cantilever (case iii), we simulated as a piece of silicon of 4 μm thickness with 125 μm length and 60 μm width. The length and width were chosen to match the tip structure of THz range simulation. As shown in Figure 4b, the addition of an Au substrate adjacent to the tip apex can greatly increase the corresponding E_{norm}, which has been validated in previous work.[10, 23] The exponential decay of E_{norm} (at 1 nm above the tip apex) with the tip-substrate distance h confirms the subwavelength-scale vertical field confinement at the tip apex (Figure S5 in the Supplemental Material).[17] Besides the intensity of the E_{norm}, essential spectral responses would also be influenced by cantilever structures. Figure 4c plots the E_{norm} spectra of case ii and iii, exhibiting a redshift of the resonant wavelength. We assign the sample-induced spectral shift to the secondary local field generated by the scattered field from the sample surface, which highly depends on the tip-substrate distance and sample dielectric properties.[24] However, for case iii, we found that

8

the Si cantilever here does not affect the major resonant wavelength compared with case ii, and also slightly increases the resonant intensity. This phenomenon can be simply explained by the pre-existing Si base, which has already induced the dominant capacitive impedance and thus reduced the interference from cantilever structure. Furthermore, the nonlinear positive correlation between the second resonance intensity and length ratio, as shown in Figure 2d and Figure 3d, remains valid within different geometric setups (Figure S6 in the Supplemental Material).[17] The scattering from the AFM tip is reported to possess strong angular dependence with the near-field resonance.[16] On account of this, we further observed that the length ratio can also influence the far-field radiation pattern, especially around the low-wavelength resonance (Figure 4d). In this range, the partially coated tip provides a better backscattering far-field signal than pure Au tip, in terms of wider angular bandwidth and higher lobe amplitude. Such enhancement from CLE becomes less obvious with larger illuminated wavelengths in accord with our earlier discussion (Figure S7 in the Supplemental Material).[17]
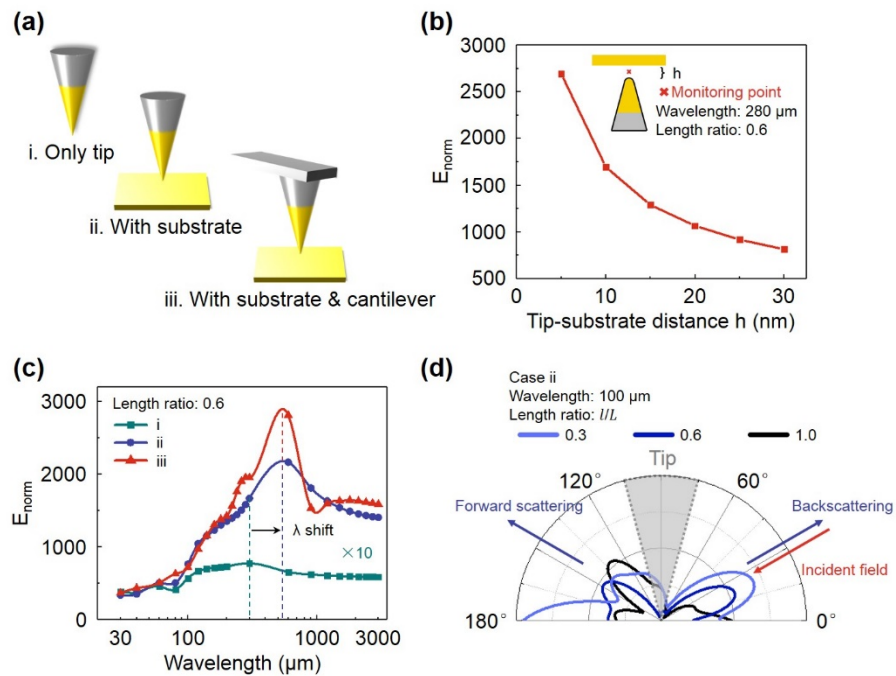

Figure 4. Simulation of the near-field enhancement with different geometry. (a) Antenna geometries considered in the simulation. i) only tip (default); ii) antenna tip with Au substrate; iii) antenna tip with Au substrate and Si cantilever. (b) Near-field intensity enhancement as a function of tip-substrate distance, for geometry ii) depicted in (a). The monitoring point is fixed at 1 nm above the tip apex, shown as the red "x" marker. The illuminated light wavelength is fixed at 280 μm and the length ratio is fixed at 0.6 (L = 200 μm). (c) The E_{norm} as a function of illuminating light wavelength for all geometries depicted in (a). The tip-substrate distance is 10 nm and the length ratio is fixed at 0.6 (L = 200 μm). The spectra of geometry i) is scaled by a factor of 10 for better visibility. (d) The scattered far-field distribution with different length ratios for geometry ii) depicted in (a). The tip-substrate distance is 10 nm and the illuminated light wavelength is fixed at 100 μm.

So far, we have discussed the CLE of standard cone shape coating for near-field nanospectroscopy. Additionally, we further study the CLE of the chiral AFM probe, as shown in Figure 5a. Recent works have demonstrated the chiral nanostructure on AFM tip can introduce unique near-field optical interaction, such as the enantioselective optical forces and handedness-sensitive near-field enhancement.[13, 26] However, most of these researches appear in ultra-violet and visible light range, which cannot address plasmonic field enhancement of dichroism (vibrational circular dichroism) in the mid-infrared range.[27-29] Here, we changed the cone-shape coating into a chiral structured coating on the same bare Si base (20 μm total length), and preserved the CLE by tuning the width l of Au ring within each fixed period distance L. Therefore, we can change the chirality of the AFM tip in the mid-infrared range by tuning the length ratio ($\frac{l}{L}$). To elucidate the variations of the near-field enhancement for different length ratios, we first assume a right-handed coating direction with left- (L-) and right- (R-) circularly polarized light (CPL) illumination. Figure 5b shows the near-field enhancement mapping of the R-chiral tip under R-CPL light (E_{R-CPL}), proving the coating ratio can still affect the near-field responses under CPL light.

Notably, the chiral tip would enhance the electrical near-field for both CPL; only that the enhancement factor is different. To illustrate this, we simulate the mapping of the R-chiral tip under L-CPL light (E_{L-CPL}), and divide the E_{R-CPL} by E_{L-CPL} to quantitatively evaluate the relationship between structural chirality and light handedness. Figure 5c shows the mapping of near-field enhancement with CPL derivatives. For a fixed illuminating light wavelength, the $\frac{E_{R-CPL}}{E_{L-CPL}}$ ratio does not always larger than 1 for the R-chiral tip, but fluctuates as the coating ratio increases (Figure 5d). This is due to the intricate spatial match between the chiral geometry and CPL wavelength, which depends the enantiomeric near-field enhancement. In particular, one CPL handedness matches more with one kind of tip chirality than the other CPL derivative, whereas this matching depends on the light wavelength and length ratio. For instance, the tip with length ratio of 0.5 matches with 6 μm R-CPL more than L-CPL, while the length ratio of 0.6 is the opposite, leading to the inverse enhancement. Similar fluctuating optical responses are widely studied in circular dichroism spectra of chiral materials and metamaterials.[30-32] We have also verified this phenomenon by simulating the L-chiral tip with the same setup, and obtained the almost symmetric results (Figure S8 in the Supplemental Material).[17] Furthermore, we change the s-SNOM light setup to directly illuminated CPL (from tip apex to base) to extended the applicable situation for CLE. Figure S9 in the Supplemental Material shows the mapping of near-field enhancement with CPL derivatives.[17] Although the specific E_{norm} mapping has some differences compared with the situation of the oblique incident light, the principle behind is the same that the CLE can affect the near-field CPL responses and introduce designable chirality to the scanning tip system. These findings disclose the capabilities and importance of CLE in tuning the tip chirality and improving the CPL interaction. Nevertheless, the structural mismatch between coating and light wavelength eventually becomes prominent when the wavelength increases.

Hence, for large wavelength (>12 μm) in contrast with 20 μm tip, the fluctuation would decrease and $\frac{E_{R-CPL}}{E_{L-CPL}}$ ratio would reach to 1, as shown in Figure 5e.
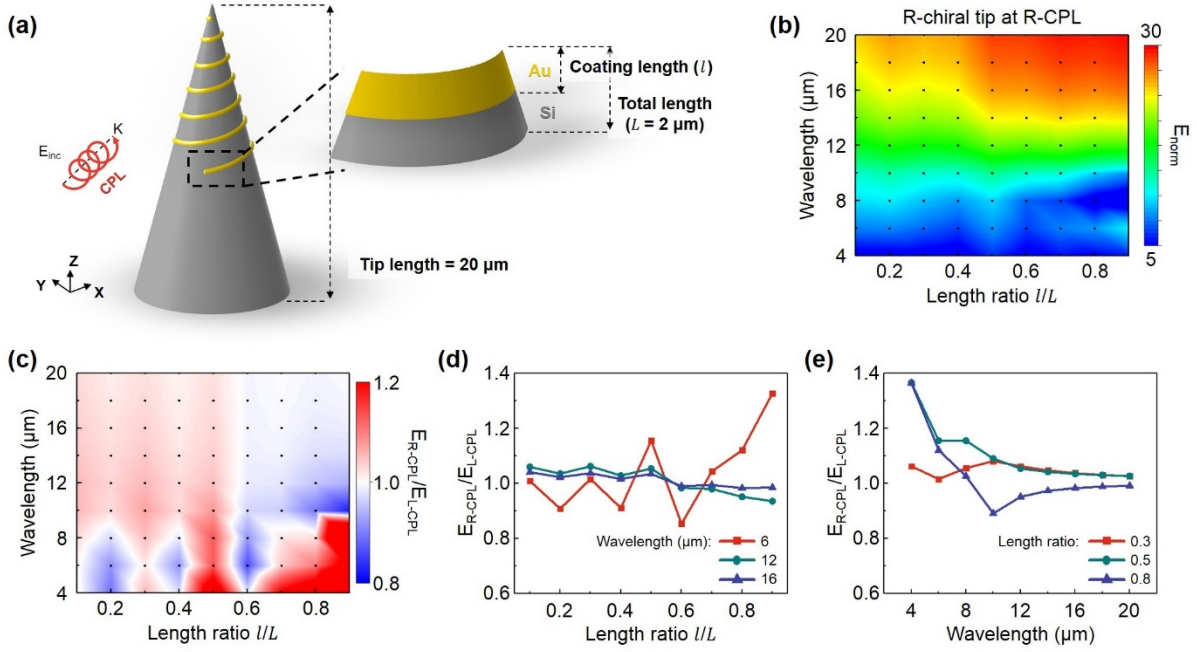

Figure 5. Numerical modeling of the chiral probe based on partially coated AFM tip for near-field CPL enhancement and differentiation. (**a**) Schematic of the numerical model to simulate the chiral tip. Au with different coating length deposit on an achiral bare Si base in a right-handed chiral (R-chiral) helical pattern, pointing from bottom to the top. The period distance (total length, L) between the center of each lap is fixed at 2 μm, while the coating length (l) varies from 0.1 to 1.9 μm. The Si base is the same as the aforementioned mid-IR setup, with 20 μm tip length and apex geometry. CPL in mid-IR range with different chirality illuminates the tip at a 60-degree angle with respect to the tip axis. (**b**) The numerically calculated near-field enhancement mapping for different length ratios and different wavelengths. The E_{norm} is calculated at 20 nm above the R-chiral tip apex which is illuminated by R-CPL. (**c**) The near-field enhancement mapping for the ratio of E_{norm} under R-CPL and L-CPL. (**d**) The horizontal line cuts of the ratio mapping, showing the E_{R-CPL}/E_{L-CPL} as a function of length ratio with different illuminating light wavelengths. (**e**) The vertical line cuts of the mapping, showing the E_{R-CPL}/E_{L-CPL} as a function of illuminating light wavelength with different length ratios.

Conclusion

In summary, we have performed numerical simulations to study the CLE on conventional AFM tips in a broad spectral range. The partially coated tips were found to yield a better tip-enhancement at certain IR and THz frequencies comparing to the fully coated tips. Particularly, the effective coupling with 2-10 μm and 30-100 μm light at a lower Au coating ratio would greatly surpass standard pure Au-coated or Si AFM tips. This is likely to yield a higher near-field detection signal for near-IR and multi-THz s-SNOM. We furthermore extend the CLE to the chiral tips, revealing the outstanding customizability of the tip chirality and distinct handedness-sensitive

CPL responses. Such partially–metal-coated tips can be fabricated by several nanofabrication technologies, including but not be limited to low-energy focused ion-beam deposition/etching, shadow-mask deposition, metal lift-off process, and other high-resolution metal deposition techniques.[9, 13] In this work, we mainly focused on the electric field enhancement under the AFM tip, which could be extended to the demodulated higher harmonics (S_2 signal, S_3 signal, ...) with improved simulation power.[14] In the future, the coating material can also be extended to more sophisticated materials with advanced ultrafast light responses, enhanced functionality and *in situ* tunability, such as semiconductor and chiral materials with twisted structures.[33-36] Our simulation model and results highlight the importance of selecting proper coating length and guide future practical fabrication, promising intriguing applications in IR/THz s-SNOM, cryogenic near-field nanospectroscopy, and chiral material manipulation.[37-39]

Acknowledgments

Reference

[1] E.A. Muller, B. Pollard, and M.B. Raschke, Infrared Chemical Nano-Imaging: Accessing Structure, Coupling, and Dynamics on Molecular Length Scales, J. Phys. Chem. Lett. **6**, 1275-1284 (2015).

[2] X. Chen, D. Hu, R. Mescall, G. You, D.N. Basov, Q. Dai, and M. Liu, Modern Scattering-Type Scanning Near-Field Optical Microscopy for Advanced Material Research, Adv. Mater. **31**, 1804774 (2019).

[3] S.N. Gilbert Corder, X. Chen, S. Zhang, F. Hu, J. Zhang, Y. Luan, J.A. Logan, T. Ciavatti, H.A. Bechtel, M.C. Martin, M. Aronson, H.S. Suzuki, S.-i. Kimura, T. Iizuka, Z. Fei, K. Imura, N.K. Sato, T.H. Tao, and M. Liu, Near-field spectroscopic investigation of dual-band heavy fermion metamaterials, Nat. Commun. **8**, 2262 (2017).

[4] M. Wächter, M. Nagel, and H. Kurz, Tapered photoconductive terahertz field probe tip with subwavelength spatial resolution, Appl. Phys. Lett. **95**, 041112 (2009).

[5] Z. Li, S. Yan, Z. Zang, G. Geng, Z. Yang, J. Li, L. Wang, C. Yao, H.-L. Cui, C. Chang, and H. Wang, Single cell imaging with near-field terahertz scanning microscopy, Cell Prolif. **53**, e12788 (2020).

[6] S.T. Chui, X. Chen, M. Liu, Z. Lin, and J. Zi, Scattering of electromagnetic waves from a cone with conformal mapping: Application to scanning near-field optical microscope, Phys. Rev. B **97**, 081406 (2018).

[7] Y. Luan, L. McDermott, F. Hu, and Z. Fei, Tip- and Plasmon-Enhanced Infrared Nanoscopy for Ultrasensitive Molecular Characterizations, Phys. Rev. Appl. **13**, 034020 (2020).

[8] S.T. Huntington and S.P. Jarvis, Application of carbon nanotubes to topographical resolution enhancement of tapered fiber scanning near field optical microscopy probes, Rev. Sci. Instrum. **74**, 2933-2935 (2003).

[9] F. Huth, A. Chuvilin, M. Schnell, I. Amenabar, R. Krutokhvostov, S. Lopatin, and R. Hillenbrand, Resonant Antenna Probes for Tip-Enhanced Infrared Near-Field Microscopy, Nano Lett. **13**, 1065-1072 (2013).

[10] S. Mastel, M.B. Lundeberg, P. Alonso-González, Y. Gao, K. Watanabe, T. Taniguchi, J. Hone, F.H.L. Koppens, A.Y. Nikitin, and R. Hillenbrand, Terahertz Nanofocusing with Cantilevered Terahertz-Resonant Antenna Tips, Nano Lett. **17**, 6526-6533 (2017).

[11] C. Ropers, C.C. Neacsu, T. Elsaesser, M. Albrecht, M.B. Raschke, and C. Lienau, Grating-Coupling of Surface Plasmons onto Metallic Tips: A Nanoconfined Light Source, Nano Lett. **7**, 2784-2788 (2007).

[12] V. Lotito, U. Sennhauser, C. Hafner, and G.-L. Bona, Fully Metal-Coated Scanning Near-Field Optical Microscopy Probes with Spiral Corrugations for Superfocusing under Arbitrarily Oriented Linearly Polarised Excitation, Plasmonics **6**, 327-336 (2011).

[13] Y. Zhao, A.A.E. Saleh, M.A. van de Haar, B. Baum, J.A. Briggs, A. Lay, O.A. Reyes-Becerra, and J.A. Dionne, Nanoscopic control and quantification of enantioselective optical forces, Nat. Nanotechnol. **12**, 1055-1059 (2017).

[14] X. Chen, C.F.B. Lo, W. Zheng, H. Hu, Q. Dai, and M. Liu, Rigorous numerical modeling of scattering-type scanning near-field optical microscopy and spectroscopy, Appl. Phys. Lett. **111**, 223110 (2017).

[15] F. Mooshammer, M.A. Huber, F. Sandner, M. Plankl, M. Zizlsperger, and R. Huber, Quantifying Nanoscale Electromagnetic Fields in Near-Field Microscopy by Fourier Demodulation Analysis, ACS Photonics **7**, 344-351 (2020).

[16] P. McArdle, D.J. Lahneman, A. Biswas, F. Keilmann, and M.M. Qazilbash, Near-field infrared nanospectroscopy of surface phonon-polariton resonances, Phys. Rev. Research 2, 023272 (2020).

[17] See Supplemental Material at [], which contains detailed information of the CLE and additional results for different partially metal-coated tips.

[18] C. Maissen, S. Chen, E. Nikulina, A. Govyadinov, and R. Hillenbrand, Probes for Ultrasensitive THz Nanoscopy, ACS Photonics **6**, 1279-1288 (2019).

[19] D.C. Adams, S. Inampudi, T. Ribaudo, D. Slocum, S. Vangala, N.A. Kuhta, W.D. Goodhue, V.A. Podolskiy, and D. Wasserman, Funneling light through a subwavelength aperture with epsilon-near-zero materials, Phys. Rev. Lett. **107**, 133901 (2011).

[20] L. Novotny, Effective Wavelength Scaling for Optical Antennas, Phys. Rev. Lett. **98**, 266802 (2007).

[21] A. Alù and N. Engheta, Input Impedance, Nanocircuit Loading, and Radiation Tuning of Optical Nanoantennas, Phys. Rev. Lett. **101**, 043901 (2008).

[22] C.A. Balanis, *Antenna theory: analysis and design*. (Wiley, 2016).

[23] A. Alù and N. Engheta, Tuning the scattering response of optical nanoantennas with nanocircuit loads, Nat. Photonics **2**, 307-310 (2008).

[24] L. Novotny and B. Hecht, *Principles of nano-optics*. (Cambridge university press, 2012).

[25] M.S. Anderson, Locally enhanced Raman spectroscopy with an atomic force microscope, Appl. Phys. Lett. **76**, 3130-3132 (2000).

[26] M. Kamandi, M. Albooyeh, M. Veysi, M. Rajaei, J. Zeng, H.K. Wickramasinghe, and F. Capolino, Unscrambling Structured Chirality with Structured Light at the Nanoscale Using Photoinduced Force, ACS Photonics **5**, 4360-4370 (2018).

[27] M. Parrinello and A. Rahman, Crystal Structure and Pair Potentials: A Molecular-Dynamics Study, Phys. Rev. Lett. **45**, 1196-1199 (1980).

[28] R. Knipper, T.G. Mayerhöfer, V. Kopecký, U. Huebner, and J. Popp, Observation of Giant Infrared Circular Dichroism in Plasmonic 2D-Metamaterial Arrays, ACS Photonics **5**, 1176-1180 (2018).

[29] F. Mattioli, G. Mazzeo, G. Longhi, S. Abbate, G. Pellegrini, E. Mogni, M. Celebrano, M. Finazzi, L. Duò, C.G. Zanchi, M. Tommasini, M. Pea, S. Cibella, R. Polito, F. Sciortino, L. Baldassarre, A. Nucara, M. Ortolani, and P. Biagioni, Plasmonic Superchiral Lattice Resonances in the Mid-Infrared, ACS Photonics **7**, 2676-2681 (2020).

[30] J. Yeom, B. Yeom, H. Chan, K.W. Smith, S. Dominguez-Medina, Joong H. Bahng, G. Zhao, W.-S. Chang, S.-J. Chang, A. Chuvilin, D. Melnikau, A.L. Rogach, P. Zhang, S. Link, P. Král, and N.A. Kotov, Chiral templating of self-assembling nanostructures by circularly polarized light, Nat. Mater. **14**, 66-72 (2015).

[31] Y. Gao, S. Kaushik, E.J. Philip, Z. Li, Y. Qin, Y.P. Liu, W.L. Zhang, Y.L. Su, X. Chen, H. Weng, D.E. Kharzeev, M.K. Liu, and J. Qi, Chiral terahertz wave emission from the Weyl semimetal TaAs, Nat. Commun. **11**, 720 (2020).

[32] Z. Wu, X. Chen, M. Wang, J. Dong, and Y. Zheng, High-Performance Ultrathin Active Chiral Metamaterials, ACS Nano **12**, 5030-5041 (2018).

[33] E. Sakat, V. Giliberti, M. Bollani, A. Notargiacomo, M. Pea, M. Finazzi, G. Pellegrini, J.-P. Hugonin, A. Weber-Bargioni, M. Melli, S. Sassolini, S. Cabrini, P. Biagioni, M. Ortolani, and L. Baldassarre, Near-Field Imaging of Free Carriers in ZnO Nanowires with a Scanning Probe Tip Made of Heavily Doped Germanium, Phys. Rev. Appl. **8**, 054042 (2017).

[34] X. Lin, Z. Liu, T. Stauber, G. Gómez-Santos, F. Gao, H. Chen, B. Zhang, and T. Low, Chiral Plasmons with Twisted Atomic Bilayers, Phys. Rev. Lett. **125**, 077401 (2020).

[35] T. Stauber, T. Low, and G. Gómez-Santos, Chiral Response of Twisted Bilayer Graphene, Phys. Rev. Lett. **120**, 046801 (2018).

[36] Y. Cheng, W. Li, and X. Mao, Triple-Band Polarization Angle Independent 90° Polarization Rotator Based on Fermat's Spiral Structure Planar Chiral Metamaterial, Prog. Electromagn. Res. **165**, 35-45 (2019).

[37] Y. Zhang and T.H. Tao, Skin-Friendly Electronics for Acquiring Human Physiological Signatures, Adv. Mater. **31**, 1905767 (2019).

[38] C. He, Z. Feng, S. Shan, M. Wang, X. Chen, and G. Zou, Highly enantioselective photo-polymerization enhanced by chiral nanoparticles and in situ photopatterning of chirality, Nat. Commun. **11**, 1188 (2020).

[39] X. Chen, X. Fan, L. Li, N. Zhang, Z. Niu, T. Guo, S. Xu, H. Xu, D. Wang, H. Zhang, A.S. McLeod, Z. Luo, Q. Lu, A.J. Millis, D.N. Basov, M. Liu, and C. Zeng, Moiré engineering of electronic phenomena in correlated oxides, Nat. Phys. **16**, 631-635 (2020).